12th U. S. National Combustion Meeting
Organized by the Central States Section of the Combustion Institute
May 24–26, 2021 (Virtual)
College Station, Texas

Concurrent-Flow Flame Spread in a Narrow Flow Duct in Microgravity – Effects of Flow Confinement and Radiation Reflection

Yanjun Li[1], Ya-Ting T. Liao[1], Paul V. Ferkul[2], Michael C. Johnston[2]*

[1]Case Western Research University, 10900 Euclid Avenue. Cleveland Ohio, 44106, USA
[2]NASA Glenn Research Center, Cleveland, Ohio, 44135, USA
[*]Corresponding Author Email: yating.liao@case.edu

Abstract: Three-dimensional numerical study is performed to investigate concurrent-flow flame spread over thin solid fuels in microgravity. The model considers the burning scenarios of a recently concluded ISS microgravity experiment, Confined Combustion. Cellulose based thin samples are burned in a small flow duct. The height of the flow duct and the radiation reflectance of the duct wall are varied. Flame development and steady spread flame characteristics are compared to the experimental results at various duct heights for validation. The numerical results demonstrate that the confinement imposed by the duct walls accelerates the flow during the combustion thermal expansion, enhancing the conductive heat transfer to the solid samples. However, when the duct height is below a critical height, the flow confinement limits oxygen supply to the flame, and the duct wall acts as a conductive heat sink. As a result of the interplay of all these effects, the flame spread rate and pyrolysis length first increase and then decrease as the duct height decreases. Eventually, the flame fails to spread at a quenching duct height. In addition, special finger shaped flamelets are observed below the critical duct height. This special flame shape increases the flame surface area and facilitates oxygen transport to the combustion zone. When the duct wall reflectance varies, higher reflectance yields a longer pyrolysis length and a faster flame spread rate. This is due to enhanced heat input to both the solid sample surface and the gaseous flame. This effect is most significant for medium duct heights. At large duct heights, the duct wall is far away from the flame and the sample. At small duct heights, while flame spread rate increases with the wall reflectance, the pyrolysis and flame length remain similar as the combustion is limited by oxygen supply.
Keywords: microgravity combustion; concurrent-flow flame spread; radiation reflection; flow confinement.

1. Introduction

Fires in confined spaces can exhibit very different behaviors from fires in open spaces and can be more dangerous [1]. In 2019, 55% of fires in the US occurred in confined structures (e.g., residential buildings, vehicles) and accounted for 98% of the total property loss [1]. In many recent fire accidents of the high-rise buildings (e.g., Grenfell tower fire in 2017), confinement imposed by external structures on building façade was identified to contribute to the fast fire growth [2]. To address this concern, this work aims to study fire behaviors and flame spread in confined spaces. Specifically, the interactions between a spreading flame and its surrounding

walls and effects of such interactions on flame characteristics (e.g., flame length, spread rate, flame shape) will be examined through numerical simulations.

Many past studies have focused on the mechanical (or aerodynamic) interactions between structures and fire, using stationary burners in rooms, corners, tunnels, or near walls [3, 4, 5]. Many other studies have focused on tunnel fires with ventilated flows [6, 7]. In most of these studies, fires are simulated experimentally using stationary burners – the flame does not move. However, fires in most real scenarios involve flames that themselves move or spread across the fuel. Flame spread is one of the most important characteristics of a fire, as it determines the available time to control the fire or to escape the area.

Upward flame spread in open and confined spaces has been studied in many previous work [5, 8, 9]. It is commonly acknowledged to be an accelerating process – both the rate of fire spread and the length of the flame continually increase. From a safety point of view, this acceleratory nature is dangerous. It is generally unknown if upward-spreading flames would eventually approach a steady-state spread rate and a limiting length, because it is impractical to construct an experimental apparatus tall enough to address this problem. Buoyancy has a major influence on fire growth processes in normal gravity and may mask observation of the fundamental underlying physics. In addition, soot radiation, which increases with fire size, further complicates the problem.

In a microgravity environment, buoyancy is essentially eliminated so that forced flow can be imposed on the sample independent of other parameters. Rather than being classified as upward (or in a particular direction), flame spread in microgravity is defined as concurrent-flow or opposed-flow depending on its direction relative to the flow. Note that on earth, upward flame spread is concurrent-flow as the flame spreads in the same direction as the buoyancy-driven flow.

For concurrent-flow flame spread in microgravity, limiting flame lengths and steady spread rates were predicted by numerical models for thin and thick samples [10, 11]. The steady spread and limiting flame length have been verified experimentally in space where thick plastic rods [12] and thin fabric samples [13] were burned in low-speed concurrent flows in a small duct aboard the International Space Station (ISS). In a recent NASA project (Saffire), a series of large-scale flame spread experiments were conducted in unmanned space vehicles [14, 15]. The sample and flow duct in in these experiments had a dimension of one order magnitude larger than prior experiments. Results yielded significantly slower flame spread rates than seen in previous smaller-scale experiments for the same samples, even when all other environmental conditions were the same (oxygen, pressure, and flow speed). This demonstrates that the confinement can have significant effects on the flame spread characteristics.

Several research groups conducted numerical studies to investigate similar situations [16, 17, 18, 19, 20]. For instance, Shih and T'ien used a steady two-dimensional model to study concurrent-flow flame spread over thin solids in a flow tunnel in microgravity. Their results showed that the flame spread rate increases as the tunnel height decreases [16], consistent with the experimentally observed phenomenon. However, when the tunnel height is very small, their results showed that conductive heat loss to the tunnel walls increases, slowing the spread rate.

This eventually leads to flame quenching. Their results also showed that for the same tunnel height, the flame becomes longer, and the spread rate increases when the reflectivity of the tunnel wall increases. No steady state solution was achieved for wall reflectivity close to one. This may indicate that flame continues to grow when subjected to radiation reflection from the tunnel wall. Such transient process cannot be captured by a steady state model.

Similar process was studied by Li et al using a three-dimensional transient numerical model [19, 20]. In their work, tunnel walls were simulated as black surfaces (no radiation reflection). Steady state was achieved in most of the simulated cases (except when the duct height is close to the quenching limit). The steady state flame spread rate first increases and then decreases when the tunnel height decreases. When the tunnel height was reduced to near the quenching height, the transient model of Li et al captured an oscillating flame: flame length, reaction intensity, and maximum flame temperature oscillated with time before flame quenched.

Shih [17] and Malhotra et al [18] simulated respectively concurrent [17] and opposed [18] flow flame spreads over parallel thin solid fuel sheets in microgravity using steady two-dimensional models. The fuel sheets were oriented parallel to the flow direction. The flow confined between adjacent sheets is similar to flow in a tunnel. At first, as the fuel sheets are brought together, the spread rate increases as the separation distance decreases. For intermediate fuel-sheet-separation distances, no steady solutions were obtained unless there was no radiation interaction between the flame and the fuel. When the separation distance is further decreased, the flame spread rate decreases and eventually the flame quenches due to flow resistance, limited thermal expansion, and oxygen starvation.

These numerical studies suggest that flow confinement and radiation reflection play important roles on the burning behaviors of solid combustibles (steady, continuously growing, or quenching). They also affect the characteristics of flame spread (flame length and spread rate). To further elaborate the effects of confinement on flame spread, Li et al conducted microgravity experiments aboard the International Space Station (ISS) [21]. In their project, Confined Combustion, thin cotton-blend fabrics were burned in concurrent flows in a flow duct. To create different levels of confinement, two flow baffles were placed parallel next to the sample, one on each side symmetrically. Different levels of radiation reflection were imposed by using three different types of baffles, black anodized and polished aluminum and transparent polycarbonate baffles. Flow speeds and sample-baffle distance were also varied. At high flow speeds (> 15 cm/s), Li et al observed an accelerating flame: flame length and flame spread rate continuously grew throughout the test. When the flow speed was reduced (e.g., 6 cm/s), flame reached a steady state with a constant spread rate. The steady flame spread rate increases first and then decreases when the baffle distance decreases. When comparing between the three different types of baffles, flame spread rate was highest for the polished baffles and lowest for the transparent baffles.

Confined Combustion was the first to examine the combined effects of flow confinement and radiation reflection on concurrent-flow flame spread in microgravity. While qualitative discussions were given, it was challenging to discuss such effects quantitatively. As in many other microgravity experiments, number of test points and diagnostics are limited. In addition,

the spectral radiation properties of the baffles were hard to control, adding complexity when interpreting the results.

The objective of this work is to further investigate the interplay of the flow confinement and radiation reflection and their combined effects on flame characteristics. This is achieved through a three-dimensional transient numerical study. The geometry and burning scenarios are based on the Confined Combustion experiments [21]. The height of the flow duct and the radiation reflectance are systematically varied. The detailed profiles of the gas and solid phases, including the gas temperature, reaction contour, and heat fluxes on the sample surface, are compared between different cases. The results are also compared with Confined Combustion experiment data.

2. Numerical model description

The numerical model used in this work is based on a three-dimensional transient Computational Fluid Dynamic (CFD) in-house program. This model has been proven robust and validated against experimental data in a wide range of oxygen and flow conditions [13, 14].

The model simulates the gaseous flame and the solid fuel sample. In the gas phase, the combustion and transport processes are simulated using direct numerical simulation. Three-dimensional transient Navier-Stokes equations are solved for the conservation of mass, momentum, energy, and species. One-step, second-order, finite rate global Arrhenius kinetics is assumed for the gas-phase reaction. Radiation Transfer Equation is also solved for gas radiation. In the solid phase, the mass and energy conservation equations are solved for the fuel sample and the sample holder. A two-step in-depth pyrolysis model is applied for the thermal decomposition of the sample fuel [13]. Grey diffusive surface radiation is considered on the surface of the sample and sample holder. The gas and solid phases are coupled to each other through interfacial boundary conditions. More detailed model descriptions, including theoretical formulation, gas and solid properties, mesh arrangement, time marching schemes, and numerical parameters can be found in previous papers [13, 22, 23].

The model configuration in this work is shown in Fig. 1. A thin solid sample (a cotton-blend, consisting of 75% cotton and 25% non-combustible fiberglass) is mounted on a sample holder and is positioned in the center of a flow duct. A uniform air flow of 6 cm/s is imposed at the duct inlet. Ignition of the sample is achieved by applying an external heat flux on the upstream leading edge of the sample. After ignition (defined when the maximum gas temperature exceeds 1500K), the external heat flux is removed. The simulation conditions are in zero gravity, with ambient pressure of 1 atm and ambient temperature of 300K.

The model configuration and the sample selection are based on the ISS project, Confined Combustion [21]. Dimensions corresponding to Confined Combustion are first simulated (Figure 1b). This allows direct comparisons between the modeling and experimental results (discussed in Chapter 3). After the model is validated against the experimental data, parametric studies are performed against flow duct height and the duct ceiling reflectance. In the parametric studies (discussed in Chapter 4), the height of the flow duct (H) varies between 1.5 cm and 15.0 cm. Longer lengths of the flow duct and fuel sample are used compared to the experiments

(dimensions listed in Figure 1c). This is to allow sufficient time (and distance) for the flame development and to facilitate the observation of the steady spreading flame.

In all simulations, symmetry boundary conditions are applied on the plane along the sample center line ($z = 0$, referred to as the center plane hereafter) and on the plane of half sample thickness. This reduces the computational domain to a quarter (marked by the green box in Figure 1a).

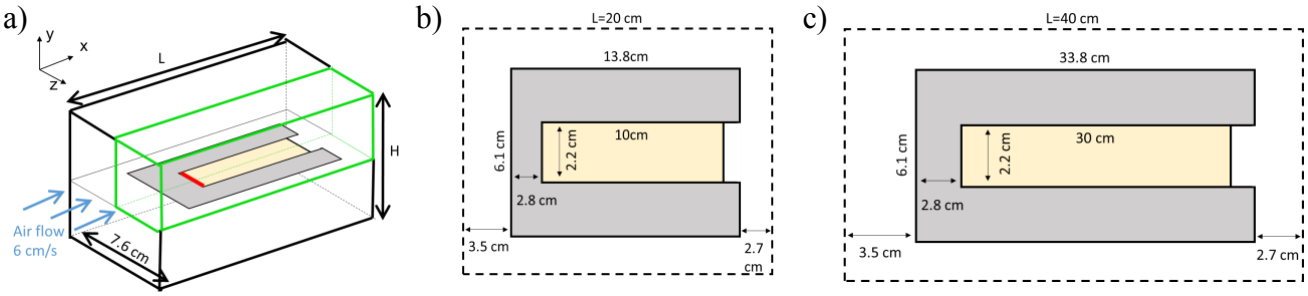

Figure 1. Model configuration (not to scale). a) Sample, sample holder, and the flow duct. b) Sample dimensions used in the model validation. c) Sample dimensions used in parametric studies on duct height and duct ceiling radiation reflection.

Constant temperature of 300K is assumed on all duct walls. The duct ceiling ($y = H/2$, the wall parallel to the sample) is assumed to be gray diffusive (radiation heat transfer is independent of wavelength and directions). The radiative reflectance (ρ) of the duct ceiling varies between 0 (black surface) and 1.0 (fully-reflecting surface). The duct side wall ($z = 3.8$ cm, the wall perpendicular to the sample surface) is assumed to be black surface.

All simulations are performed on the Case High Performance Computing Cluster at Case Western Reserve University. The total mesh ranges from 476k – 810k and the simulations typically take ~120 to 226 hours with parallel computing using 12 processors.

3. Validation against microgravity experiments

3.1 Transient flame growth process

In all simulated cases, the flame grows initially after ignition and then reaches a limiting length and a steady spreading rate. This is consistent with the observations in Confined Combustion: flame reaches a steady state at low flow speeds. The transient flame development process is demonstrated using a representative case ($H = 5$ cm, $\rho = 0$) in Figure 2 (right panes). The modeling results are compared to a Confined Combustion test. In the test, sample was positioned between in a pair of black baffles with inter-baffle distance of 5 cm. Flame images from the experiments are shown in Figure 2 (left panes).

A reaction kernel was observed almost immediately after the ignitor was energized (time = 1 s in Figure 2). Shortly after ignition (t ~10 s), flame reached steady state and spread downstream along the sample surface. Numerical and experiment results show similar flame shapes during

the steady flame spread and the flame standoff distance (distance from the flame to the sample surface) increases in downstream direction. When the flame tip reached the end of sample (t ~ 50s), it rounded to the sample surface. This was caused by the absence of no-slip boundary condition downstream to the sample (Figure 1b). Eventually, the flame consumed all the combustibles and quenched. Figure 2 demonstrates that the numerical model captures the transient flame growth and spread progresses observed in the experiment.

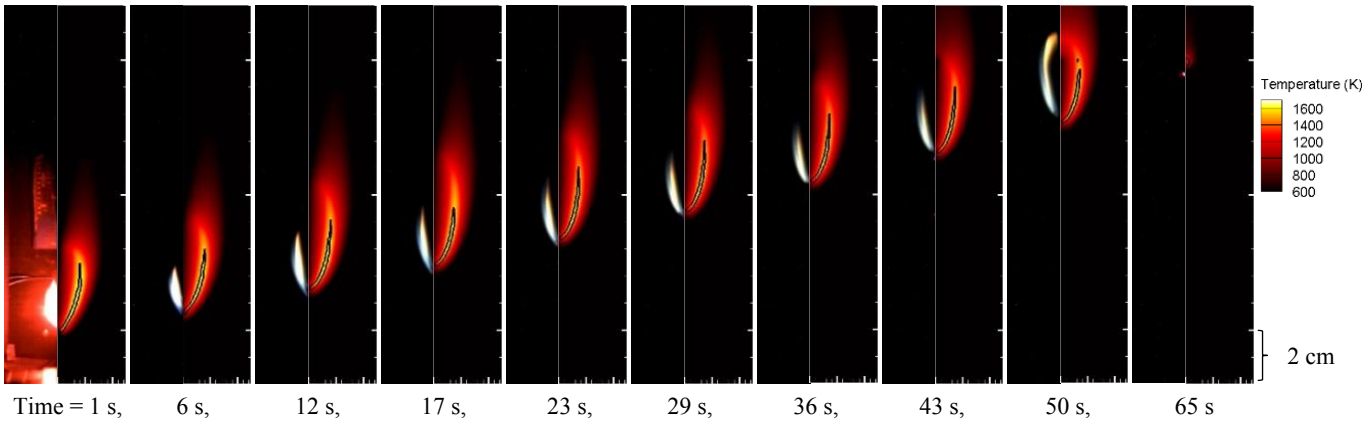

Figure 2. Comparison of the flame growth between microgravity experiment (left panes) and numerical simulation (right panes). The flame shape (black contour) in the numerical simulation is defined as the iso-line of fuel vapor reaction rate 1.0E-3 g/cm^3/s. H = 5 cm, ρ=0.

To further illustrate the flame behaviors, flame positions versus time in both numerical and experiment results are plotted in Figure 3. In the numerical simulations, flame is defined as the region where fuel reaction rate is higher than 10^{-3} g/cm^3/s. In experiments, flame profiles are extracted through image analysis using a custom MATLAB code [21]. Figure 3 shows that the model quantitatively captured the flame growth and the steady spreading state.

Notice that in the experiment results, flame tip exhibits a sudden advancement when reaching the downstream end of the sample (t ~ 45 s). This is because in the experiment, flow confinement was imposed by two parallel baffles. The baffles have the same dimensions of the sample holder and extend only 1 cm downstream to the sample trailing edge (Figure 1b). When the flame tip is near the end of the sample and is close to the baffle trailing edge, oxygen can diffuse upstream into the inter-baffle region. Fuel vapor can also transport beyond and burn outside of the baffle region. These do not occur in the numerical simulations where the confinement is directly imposed by flow duct walls.

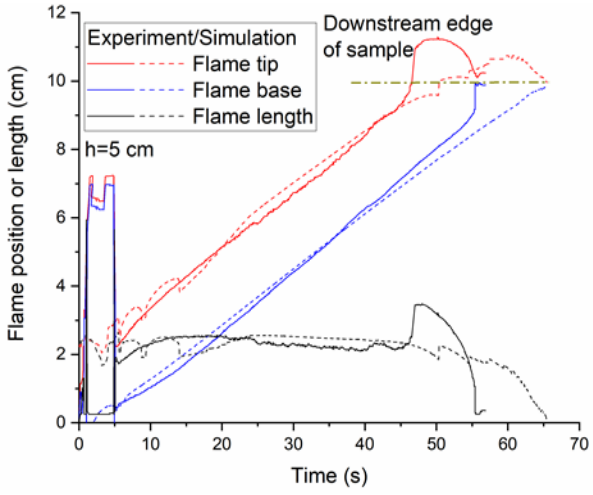

Figure 3. Flame locations and flame length versus time. H = 5 cm, ρ=0.

3.2 Flame spread rate and flame length at steady state

Steady state flame lengths and spread rates at different duct heights from experiments and from numerical modeling are compared in Figure 4. The flame spread rates are deduced from applying linear regression to the flame positions when the flame spread over the center portion of the solid fuel (4 - 7 cm). Average flame length is also deduced in the same time period.

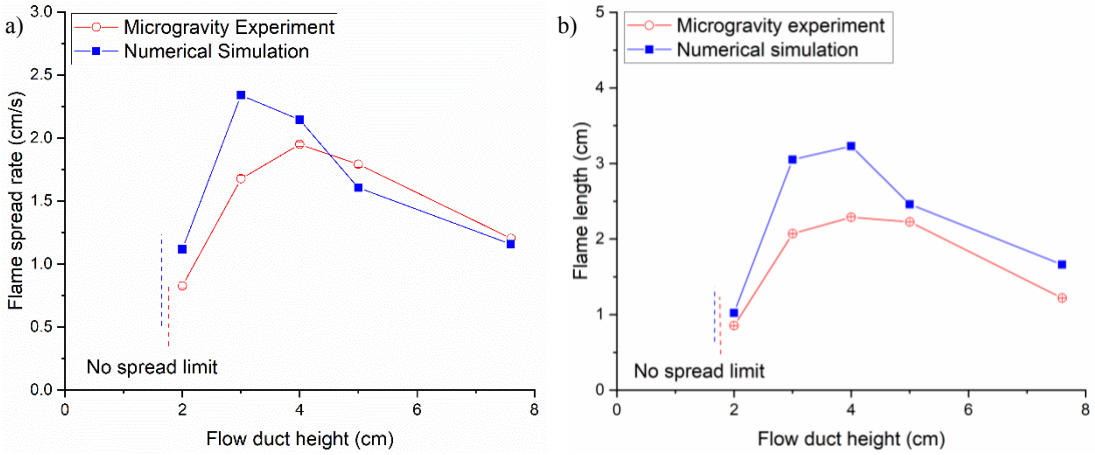

Figure 4. Flame length and spread rate at the steady state at different duct heights. ρ=0.

The numerical results are consistent with the experimental observation: the flame spread rate and flame length increase first and then decrease when the duct height decreases. This non-monotonic trend was discussed previously by Li et al [19, 20]. Three major effects of confinement were identified. The first effect is enhancement of conduction heat transfer to the

sample surface. This is through forcing the flame to stay close to the sample surface (at very small duct heights) and flow acceleration due to thermal expansion of the combustion gases. This effect increases the solid burning rate and intensifies the gas phase reaction as the duct height decreases. Second and third effects are the reduction of oxygen supply to the flame zone and introduction of heat loss to duct walls. These weaken the flame and eventually lead to a quenching duct height below which the flame fails to spread.

At large duct heights, the difference of the flame spread rate between simulation and experiment is minimal (e.g., 3.7 % difference for H= 7.6 cm). However, the difference is larger at smaller duct heights. This once again is suspected to be due to different hardware setups. In the experiments, the hardware flow characterization tests showed that flow in the inter-baffle region is lower than the imposed flow speed when the inter-baffle distance is small [21]. Friction on the sample surface and flow resistance diverted the flow to the extra-baffle region. This resulted in lower flame spread rate and flame length compared to the numerical predictions. Nevertheless, the model was able to replicate the experimentally observed effects of confinement on the flame characteristics.

4. Parametric studies on duct height and radiation reflection

4.1 Flame spread rate, flame length, and pyrolysis length

To investigate the combined effects of the duct height and the radiation reflection, pyrolysis length and flame spread rate from all simulated cases are compared in Fig. 5. The pyrolysis zone is defined as the region where solid mass burning rate exceeds 10^{-5} g/cm^2/s [22]. When ceiling reflectance is fixed (see black iso-reflectance lines), both flame spread rate and pyrolysis length increase and then decrease when the duct height increases. This remains true for all duct reflectance. At a fixed duct height (symbols of the same colors in Fig. 5), both pyrolysis length and spread rate increase when the ceiling reflectance increases. While this phenomenon is generally true for all duct heights, it is most prominent at medium simulated duct height H = 4 cm, consistent with the findings in Confined Combustion [21]. Below this duct height, the sensitivity of the pyrolysis length on the ceiling reflectance is lower than that of flame spread rate. At the smallest and largest duct heights (H = 1.5 and 15 cm), flame length and spread rate remain similar when duct ceiling reflectance varies.

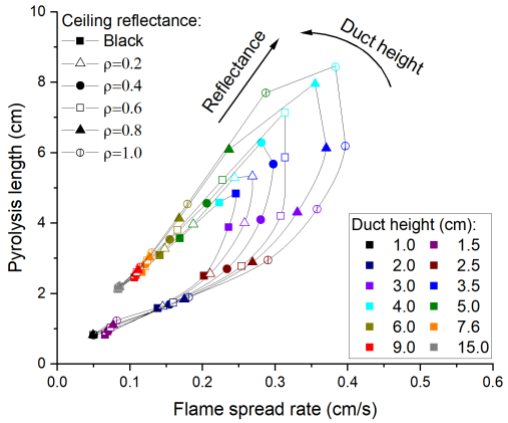

Figure 5. Steady state flame spread rate and pyrolysis length at different duct heights and radiative reflectance.

Notice that in Figure 5, at any fixed duct height, the pyrolysis length is linearly proportional to the spread rate. This phenomenon is also observed in previous experiments for concurrent flow flame spread under different flow speeds and oxygen concentrations [14, 24, 13, 25, 26].

In Figure 6, the flame and pyrolysis lengths at different flow duct heights for black (ρ=0) and reflecting (ρ=1) ceilings are compared. Compared to the black ceiling, the reflecting ceiling has a lower no-spread limit (1.5 cm vs. 1 cm). Also notice that in Fig. 6, the optimal duct height (where the maximum flame/pyrolysis lengths occur) is larger for the reflecting duct ceiling than the black ceiling (H = 4.0 and 3.5 cm respectively). Above the optimal duct height, while flame and pyrolysis lengths both increase when duct height decreases, the flame-pyrolysis length ratio remains ~1.15-1.2. Below the optimal duct height, flame and pyrolysis lengths both decrease with decreasing duct height. The flame- pyrolysis length ratio increases. These will be discussed below.

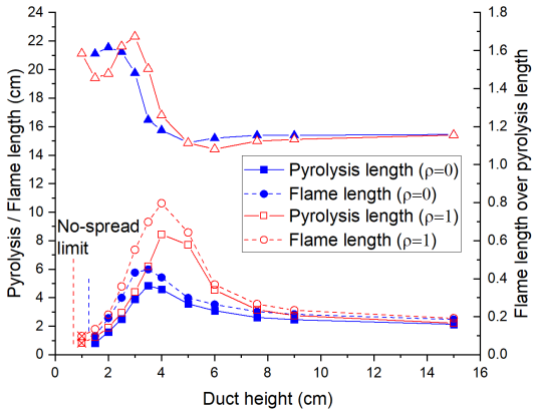

Figure 6. Flame and pyrolysis lengths at steady spreading state at different duct heights. The cross symbols denote partial flame spread.

4.2 Flame shape

The flame profiles for different duct heights are compared in Fig. 7. For large duct heights (H = 7.6 cm or H/2 = 3.8 cm), flame is far away from the ceiling. The maximum flame standoff distance is ~1 cm. The side-view flame profile (Fig. 7a Top) resembles the flow boundary layer on the sample surface, except near the downstream flame tip region. It is similar to that reported in previous work [24, 26]. For a diffusion flame spreading over a solid combustible, the fuel vapor generated on the sample surface needs to diffuse across the viscous flow boundary layer to meet the oxidizer. Near the downstream flame tip region, for a narrow sample, oxygen is able to transport (via convection and diffusion) to the sample surface from the two sides (see Fig. 7a Bottom). Hence combustion occurs near the sample surface (flame standoff distance decreases slightly near the downstream flame tip). The three-dimensional (3D) iso-surface of the reaction contour (Fig. 7a Bottom) shows that the flame has a centerline-leading profile at downstream front region (i.e., the center part of the flame travels ahead of the two sides of the flame). This centerline-leading flame shape was also reported in previous work [13, 26, 27] and was attributed to the flame heat loss to the side sample holders.

When the duct height reduces to ~3 cm (H/2 = 1.5 cm, close to the flame standoff distance), flame extends to the ceiling resulting in a blockage of oxygen to the downstream region (Fig. 7b). This duct height is slightly below the optimal duct height where the flame length has a maximum value (Fig. 6). This oxygen blockage has a profound impact on the flame shape. The 3D flame profile (Fig. 7b Bottom) shows that the flame has reversed shapes of the downstream flame front. Due to the limited oxygen supply downstream to the flame, the combustion around the sample centerline is incomplete. The unburned gas fuel needs to diffuse to the sides, seeking fresh air flow. Compared with the conventional flame shaped observed for larger duct height (Fig. 7a), this side-leading concave flame front increases the flame-pyrolysis length ratio (figure 6). Furthermore, this concave flame shape yields larger surface-volume ratio of the flames, facilitating the oxygen diffusion into the reaction zone. This mechanism is similar to the near quenching finger flames [28, 29].

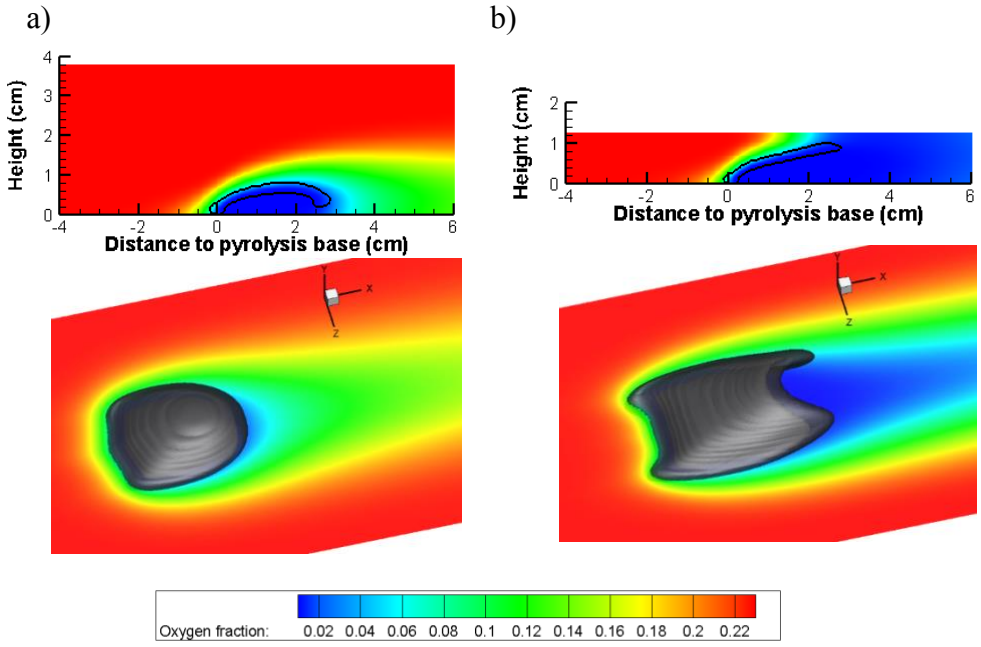

Figure 7. Effects of confinement on flame shapes. Top: Upstream flow profile (white line), mass fraction of oxygen (color contour), and flame shape (black line) on center symmetric plane. Bottom: three-dimensional iso-surface for fuel vapor reaction rate and mass fraction of oxygen near the sample surface (y = 0.2 cm). (a) H = 7.6 cm, ρ =0. (b) H = 2.5 cm, ρ =0.

4.3 Combustion efficiency

Figure 8 demonstrates the effects of the flow confinement on the total fuel vapor reaction rate and the combustion efficiency (fuel vapor reaction rate over solid fuel mass burning rate). At large duct heights, the combustion efficiency is 100% and the gas reaction rate increases when the duct height decreases. This is because of the aforementioned enhancement of conductive heat transfer to the sample surface and the resulting increased solid burning rate as the duct height reduces. When the duct height is reduced to the optimal duct height (4 cm for $\rho = 1$ and 3.5 cm for $\rho = 0$), the combustion efficiency drops below one due to the oxygen depletion. The incomplete combustion and increased heat loss to the duct ceiling both reduce flame temperature and gas burning rate as the duct height approaches the quenching duct height.

Compared to the black ceiling, the reflective ceiling is expected to result in a higher solid burning (due to the enhanced heat feedback to the solid surface). This higher solid burning rate requires more oxygen flow rate for complete combustion. Consequently, the combustion efficiency drops to below one at a higher duct height for reflective ceiling compared to the black ceiling.

Also note that, in general, the reflecting ceiling has a larger gas reaction rate. This effect is most obvious at middle duct heights. At large duct height, the sample and the flame are away from the duct ceiling. At small duct heights, the combustion is limited by the oxygen supply (ventilation-controlled). In either case, gas combustion is less sensitive to ceiling reflection.

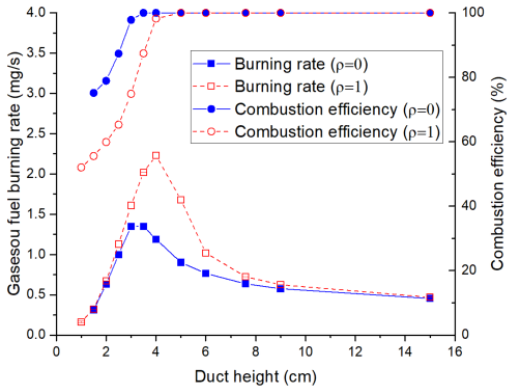

Figure 8. Fuel vapor burning rate and calculated combustion efficiency at different duct heights.

4.4 Heat flux on the sample surface

To understand the effects of the duct reflectance, the gas and solid profiles are compared between black and reflecting ceilings. For large duct heights (e.g., H = 7.6 cm, Figs. 9a and 9b), ceiling is relatively far away from the sample. For both black and reflecting ceilings, the conductive heat flux from the flame dominates in the pyrolysis region. For small duct heights (e.g., H = 2.5 cm, Figs. 9c and 9d), the upstream flame base stays closer to the sample surface and the temperature of the flame is noticeably higher compared to large duct heights. As a consequence, the conductive heat flux in small duct heights is higher compared to that of the large duct heights for both ceiling types. For the black ceiling, the duct height does not have significant effects on the radiative heat input on the sample. For the reflecting ceiling, the radiative heat flux becomes comparable to the conductive heat flux at small duct height.

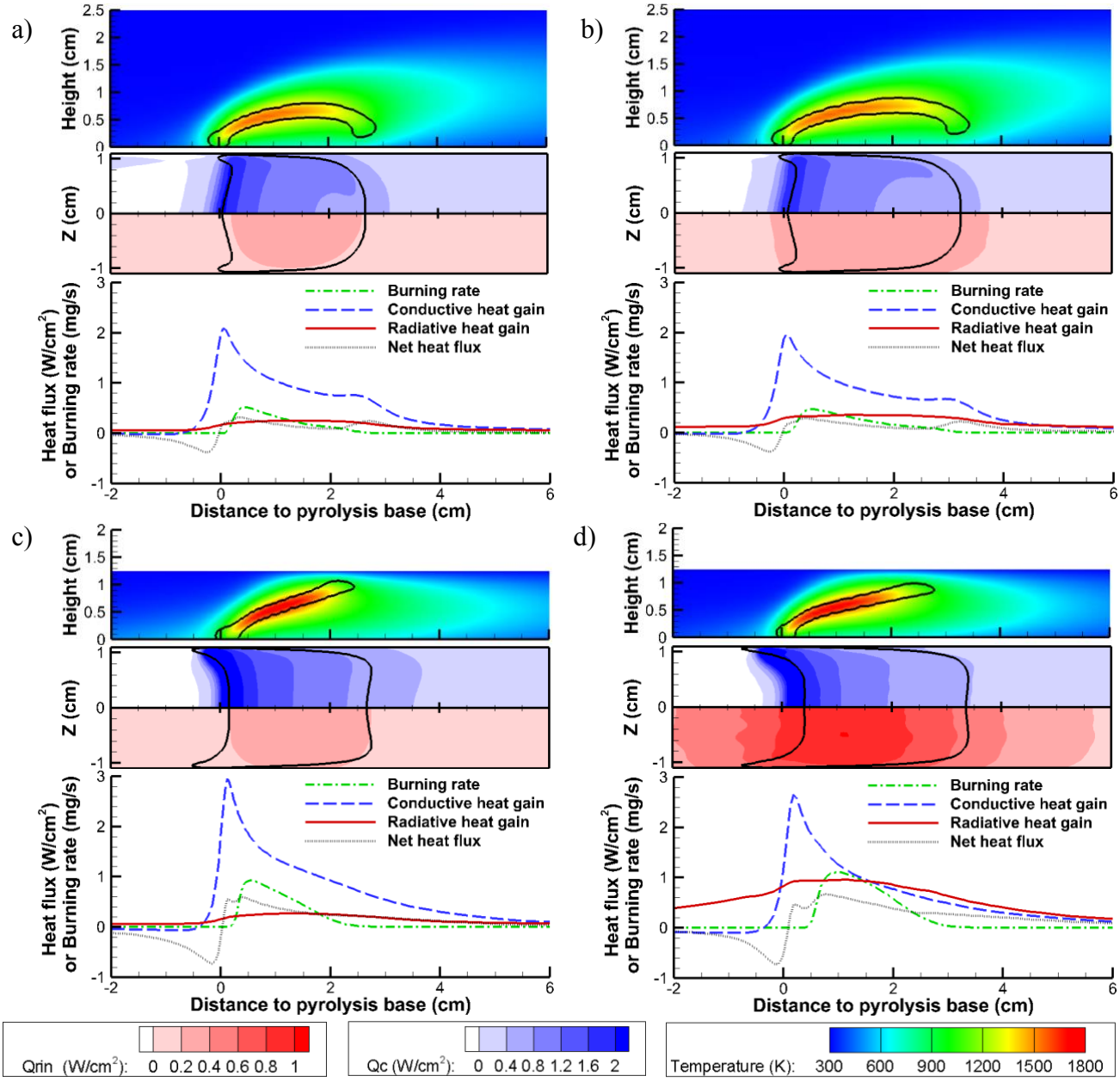

Figure 9. Gas and solid profiles. Top: flame shape (black line) and gas temperature on the center plane. Middle: conductive (blue) and radiative (red) heat flux on the sample surface. Blackline denotes the pyrolysis zone. Bottom: Heat flux distribution along the sample centerline. (a) $\rho = 0$, $H = 7.6$ cm. (b) $\rho = 1$, $H = 7.6$ cm. (c) $\rho = 0$, $H = 2.5$ cm. (d) $\rho = 1$, $H = 2.5$ cm.

The gas profile also shows an overall higher flame temperature for reflecting ceilings compared to black ceiling. This phenomenon is more obvious at small duct heights (Figs. 9c and 9d). In this simulation, the combustion products (CO_2 and H_2O) participate in the radiation transfer (i.e., emitting and absorbing radiation). It is suspected that the higher heat flux from

the reflecting ceiling also transfers more heat to the reacting gas mixture and promotes the combustion.

Also notice that, at the small duct heights, while the flame exhibits a side-leading concave front as shown in Fig. 7b, the pyrolysis front remains relatively flat across the sample width (Fig. 9c). On the sample surface profile shown in Figs. 9c and 9d, the pyrolysis front is slightly longer than the flame length on the center plane. However, the side-leading concave flame shape prolongs the overall flame length. This explains the increasing flame-pyrolysis length ratio with decreasing duct height in Fig. 6. This also leads to a larger preheat region and enhanced heat input to the solid surface.

Average conductive and radiative heat fluxes (area average) in the pyrolysis region for different cases are quantitatively compared in Fig. 10. For black ceiling (solid symbols) in all duct heights, conductive heat flux is greater than the radiative heat flux from the flame and it dominates in the solid pyrolysis process. When duct height decreases, the conductive heat flux remains constant at large duct height. When the half duct height decreases to close to the flame height, the flame is pushed towards the sample hence the conductive heat flux increases. This more condensed flame also increases the flame radiative heat flux when the height decreases. However, when the height reduces below 3.0 cm, the combustion is incomplete (Figure 8) and radiative heat flux decreased due to the reduced flame temperature compared with that at optimal duct height ~3.0 cm.

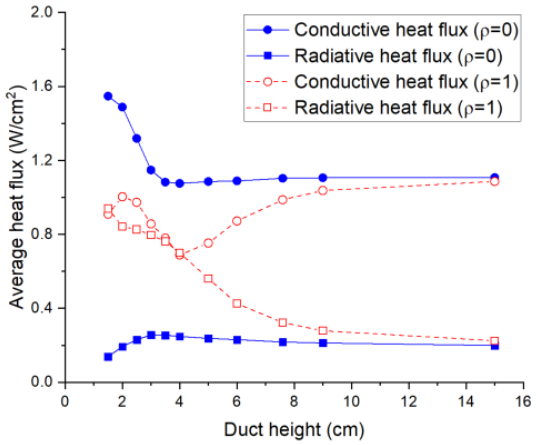

Figure 10. Average eat flux in the pyrolysis zone on the sample surface

For reflecting ceiling (open symbols in Fig. 10), the radiative heat flux is larger and conductive heat flux is smaller compared to the black ceiling. Radiative heat flux increases because the sample receives radiation from not only the flame but also the reflecting ceiling. The smaller the duct height, the greater the additional radiative heat flux the sample receives. This implies a higher sample surface temperature (confirmed in the numerical results), and hence a lower conductive heat flux compared to the results from black ceiling. At large duct heights, conductive heat transfer still dominates in the pyrolysis process for reflecting ceiling. At small duct heights, radiative and conductive heat input become compatible.

The total net heat inputs in the pyrolysis and preheat regions are compared in Fig. 11. The net heat input is the conductive and radiative heat from the flame and from the ceiling minus radiative heat loss on the sample surface. Compared to the black ceiling, the additional radiation feedback from the reflecting ceiling in general increases the net heat input to the solid surface. In the pyrolysis region, the increase of the net heat input is largest in the middle duct height (Fig. 11a). As mentioned earlier, although ceiling reflection increases the radiative heat input on the sample surface, it also increases the surface temperature and decreases the conductive heat flux. The higher sample surface temperature also results in a higher surface radiation heat loss. As the duct height decreases, this effect becomes more prominent and eventually leads to similar net heat input to the pyrolysis region for black and reflecting ceilings at small duct heights (< 2 cm). This contributes to the nearly constant pyrolysis length at small duct height when the ceiling reflectance varies (Fig. 5). In the preheat region, the effect of enhanced heating due to ceiling reflection remains even when the duct height approaches the quenching height (Fig. 11b). This explains the stronger dependency of the spread rate on the ceiling reflectance compared to the pyrolysis length at small duct heights shown in Fig. 5.

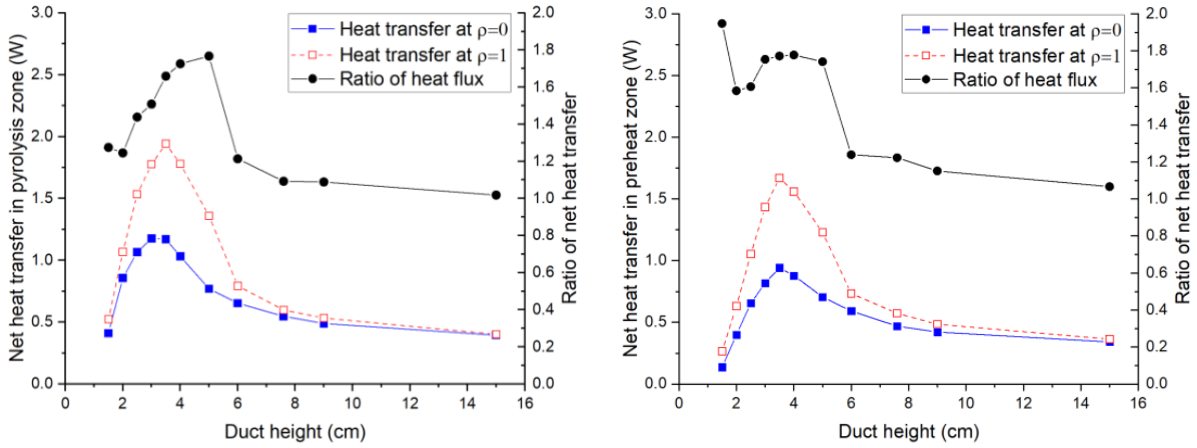

Figure 11: Net heat input on the sample surface a) in the pyrolysis region and b) in the preheat region.

5. Conclusion

Numerical studies are performed using an in-house three-dimensional transient CFD code to investigate purely forced concurrent-flow flame spread over a thin solid in a flow duct. The numerical model is shown to be able to capture the transient flame spread process and reproduce the effects of confinement on flame spread in previous microgravity experiments. The height of the flow duct and the reflectance of the duct wall are varied in the numerical investigation. Flame characteristics at the steady state between different cases are compared. The aerodynamics and thermal interactions between the flame and the duct wall are examined in detail. Key findings are as follows.

1) For any fixed wall reflectance, the flame spread rate and the pyrolysis length at steady state first increase and then decrease when the flow duct height decreases. Eventually, the flame fails to spread when a quenching duct height is reached. The flow confinement imposed by the duct has multiple effects on the flame spread process. Previous research indicates that the confinement accelerates the flow when the flow experiences thermal expansion during combustion. The duct wall also forces the flame to stay close to the sample surface, enhancing the net heat flux and local solid burning rate near the upstream flame base. These effects intensify the flame. However, at small duct heights, the confinement limits the oxygen supply to the flame in the downstream region. The flame also loses heat to the duct walls through conduction and radiation, reducing the strength of the flame. These competing effects results in the non-monotonic trend of the flame spread rate and pyrolysis length at different duct heights.
2) When the half duct height is reduced to close to the flame height, flame extends to the duct ceiling, blocking the oxygen from the downstream region. The combustion efficiency decreases as the duct height. The flame front transits from a center-leading convex shape to side-leading concave shape. This side-leading concave flame front, similar to the finger flames reported in near-quenching conditions in literature, increases the flammability in two ways. First, it increases the surface to volume ratio of the flame and facilitates the oxygen transport to the reaction zone from the two sides. Second, the flame length is extended further downstream to the pyrolysis region (i.e., flame-pyrolysis length ratio increases). This results in a larger preheat region and an enhanced heat transfer to the solid.
3) At any fixed duct height, pyrolysis length and flame spread rate generally increase with the duct ceiling reflectance. This is because the radiation reflection from the ceiling increases the net heat input in both pyrolysis and preheat region. For duct height smaller than the optimal duct height, the heat input enhancement is more pronounced in the preheat region than in the pyrolysis region. This is partly due to the increased flame-pyrolysis length ratio. As a result, at small duct heights, when ceiling reflectance increases, the flame spread rate increases but pyrolysis length remains similar. The combustion gas products (e.g., CO_2 and H_2O) also absorbs the ceiling radiation and have a higher temperature as the reflectance increases.
4) The effect of the ceiling reflectance on the flame spread process is most prominent for middle duct heights. At large duct height, the sample and the flame are away from the duct ceiling. At small duct heights, the combustion is limited by the oxygen supply (ventilation-controlled). In either case, gas combustion is less sensitive to ceiling reflection.

7. Acknowledgement

This work is supported by National Science Foundation under grant number CBET-1740478. This numerical study made use of the High Performance Computing Resource in the Core Facility for Advanced Research Computing at Case Western Reserve University.

8. References

[1] M. Ahrens and B. Evarts, "Fire Loss in the United States During 2019," National Fire Protection Association, Quincy, Massachusetts, 2020.

[2] London Fire Brigade, "London Fire Brigade Operational Response to Grenfell Tower," London Fire Brigade, London, UK, 2018.

[3] B. Y. Lattimer and U. Sorathia, "Thermal Characteristics of Fires in a Noncombustible Corner," *Fire Safety Journal,* vol. 38, pp. 709-745, 2003.

[4] M. Poreh and G. Garrad, "A Study of Wall and Corner Fire Plumes," *Fire Safety Journal,* vol. 34, pp. 81-98, 2000.

[5] K. L. Jamison and D. A. Boardman, "A New Fire Performance Test for Cavity Wall Insulation," in *MATEC Web of Conferences*, Lund, Sweden, May 13th 2016.

[6] L. H. Hu, W. Peng and R. Huo, "Critical Wind Velocity for Arresting Upwind Gas and Smoke Dispersion Induced by Near-Wall Fire in a Road Tunnel," *Journal of Hazardous Materials,* vol. 150, pp. 68-75, 2008.

[7] X. Tian, M. Zhong, C. Shi, P. Zhang and C. Liu, "Full-scale Tunnel Fire Experimental Study of Fire-induced Smoke Temperature Profiles With Methanol-Gasoline Blends," *Applied Thermal Engineering,* vol. 116, p. 233–243, 2017.

[8] M. C. Johnston, J. S. T'ien, D. E. Muff, X. Zhao, S. L. Olson and P. V. Ferkul, "Self induced buoyant blow off in upward flame spread on thin solid fuels," *Fire Safety Journal,* vol. 71, pp. 279-286, 2015.

[9] G. Markstein and J. d. Ris, "Upward fire spread over textiles," *Symposium (International) on Combustion,* vol. 14, no. 1, pp. 1085-1097, 1973.

[10] P. V. Ferkul and J. S. T'ien, "A Model of Low-Speed Concurrent Flow Flame Spread Over a Thin Fuel," *Combustion Science and Technology,* vol. 99, no. 4-6, pp. 345-370, 1994.

[11] Y.-T. Tseng and J. S. T'ien, "Limiting Length, Steady Spread, and Nongrowing Flames in Concurrent Flow Over Solids," *Journal of Heat Transfer,* vol. 132, no. 9, p. 091201, 2010.

[12] S. L. Olson and P. V. Ferkul, "Microgravity Flammability of PMMA Rods in Concurrent Flow," in *9th US National Combustion Meeting*, Cincinnati, USA, May 17th-20th, 2015.

[13] X. Zhao, Y.-T. T. Liao, M. C. Johnston, J. S. T'ien, P. V. Ferkul and S. L. Olson, "Concurrent flame growth, spread, and quenching over composite fabric samples in low speed purly forced flwo in microgravity," *Proceedings of the Combustion Institute,* vol. 36, pp. 2971-2978, 2017.

[14] C. Li and Y.-T. Liao, "Effects of Ambient Conditions on Concurrent-flow Flame Spread over a Wide Thin Solid in Microgravity," *Proceedings of the Combustion Institute,* vol. 000, pp. 1-10, 2020.

[15] D. L. Urban, P. Ferkul, S. Olson, G. Ruff, J. Easton, J. S. T'ien, Y.-T. T. Liao, C. Li, C. Fernandez-Pello, J. Torero, G. Legros, C. Eigenbrod, N. Smirnov, O. Fujita, S. Rouvreau,

B. Toth and G. Jomaas, "Flame Spread: Effects of Microgravity and Scale," *Combustion and Flame,* vol. 199, pp. 168-182, 2019.

[16] H.-Y. Shih and J. S. T'ien, "Modeling Wall Influence on Solid-Fuel Flame Spread in a Flow Tunnel," in *35th Aerospace Science Meeting & Exhibit* , Reno, NV, 1997.

[17] H.-Y. Shih, "Flame Spread and Interactions in an Array of Thin Solids in Low-Speed Concurrent Flows," *Combustion Theory and Modelling,* vol. 13, no. 3, pp. 443-459, 2009.

[18] V. Malhotra, C. Kumar and A. Kumar, "Opposed Flow Flame Spread Over an Array of Thin Solid Fuel Sheets in a Microgravity Environment," *Combustion Theory and Modelling,* vol. 17, no. 5, pp. 835-857, 2013.

[19] Y. Li, Y.-T. T. Liao and P. Ferkul, "Numerical Study of the Effects of Confinement on Concurrent-flow Flame Spread in Microgravity," *Journal of Heat Transfer,* vol. 142, no. 11, p. paper number 11301, 2020.

[20] Y. Li, Y. Liao and P. Ferkul, "Concurrent-Flow Flame Spread Over a Thin Solid in a Narrow Confined Space in Microgravity," in *International Mechanical Engineering Congress & Exposition*, Salt Lake City, USA, 2019.

[21] Y. Li, Y.-T. T. Liao, P. V. Ferkul, M. C. Johnston and C. Bunnell, "Experimental Study of Concurrent-Flow Flame Spread over Thin Solids in Confined Space in Microgravity," *Combustion and Flame,* vol. 227, pp. 39-51, 2021.

[22] Y.-T. T. Liao and J. S. T'ien, "A Numerical Simulation of Transient Ignition and Ignition Limit of a Composite Solid by a Localised Radiant Source," *Combustion Theory and Modelling,* vol. 17, no. 6, pp. 1096-1124, 2013.

[23] C. Li, Material Flammability and Burning Behavior of Thin Solids in Concurrent Forced Flow in Microgravity: A Numerical Study in Support of Large Scale Microgravity Burning Experiments, Cleveland, Ohio: Case Western Reserve University: PhD Dissertation, 2020.

[24] A.C.Fernandez-Pello, "Flame spread in a forward forced flow," *Combustion and Flame,* vol. 36, pp. 63-78, 1979.

[25] G. D. Grayson, K. R. Sacksteder, P. V. Ferkul and J. S. T'ien, "Flame spreading over a thin solid in low-speed concurrent flow- Drop tower experimental results and comparison with theory," *Microgravity Science and Technology,* vol. 7, no. 2, pp. 187-195, 1994.

[26] A. Vetturini, W. Cui, Y.-T. T. Liao, S. Olson and P. Ferkul, "Flame Spread Over Ultra-thin Solids: Effect of Area Density and Concurrent-Opposed Spread Reversal Phenomenon," *Fire Technology,* vol. 56, p. 91–111, 2020.

[27] A. Carney, Y. Li, Y.-T. Liao, S. Olson and P. Ferkul, "Concurrent-flow flame spread over thin discrete fuels in microgravity," *Combustion and Flame,* vol. 226, pp. 211-221, 2021.

[28] S. L. Olson, F. J. Miller, S. Jahangirian and I. S. Wichman, "Flame Spread over Thin Fuels in Actual and Simulated Microgravity Conditions," *Combustion and Flame,* vol. 156, no. 6, pp. 1214-1226, 2009.

[29] S. L. Olson, F. Miller and I. S. Wichman, "Characterizing fingering flamelets using the logistic model," *Combustion Theory and Modelling,* vol. 10, no. 2, pp. 323-347, 2006.